Nanoscale Advances

ROYAL SOCIETY OF CHEMISTRY

PAPER

View Article Online
View Journal | View Issue

Cite this: *Nanoscale Adv.*, 2024, **6**, 1241

Synthesis of polyoxometalate-pillared Zn–Cr layered double hydroxides for photocatalytic CO_2 reduction and H_2O oxidation†

Xiaotong Zhao, Haoyang Jiang,* Yongcheng Xiao and Miao Zhong *

Received 20th November 2023
Accepted 29th December 2023

DOI: 10.1039/d3na01024d

rsc.li/nanoscale-advances

Polyoxometalate (POM)-pillared Zn–Cr layered double hydroxides (LDHs) exhibited high photocatalytic activities in CO_2 reduction and H_2O oxidation reactions. For CO_2 reduction in pure water, the CO production was 1.17 μmol g^{-1} after a 24 h reaction. For O_2 evolution in $NaIO_3$ solution, the O_2 production reached 148.1 μmol g^{-1} after a 6 hour reaction. A mechanism study indicated that the electron transfer from Zn–Cr LDHs to POMs ($SiW_{12}O_{40}^{4-}$) promoted photocatalytic activities.

Introduction

Layered double hydroxides (LDHs) constitute a class of multifunctional materials characterized by tunable chemical compositions, featuring cationic brucite host layers and anionic interlayer guests.[1] Owing to their favorable band positions, considerable attention has been directed towards their application in photocatalytic CO_2 reduction[2–15] and oxygen evolution.[16–18] Notably, within the realm of LDHs, Zn–Cr LDHs and their derivatives have demonstrated remarkable photocatalytic properties concerning CO_2 reduction and O_2 evolution in aqueous environments. For example, Jiang *et al.*[6] observed that CO_3^{2-}-type Zn–Cr LDHs grafted with Cu_2O nanoparticles could reduce CO_2 to CO and simultaneously oxidize water to O_2.

Similarly, Hwang *et al.*[19] prepared mesoporous layer-by-layer ordered nanohybrids of Zn–Cr LDHs and layered titanate, showing improved photocatalytic O_2 generation activity. Polyoxometalates (POMs), also recognized as polyacids, represent a class of catalytically active inorganic compounds featuring highly symmetrical core assemblies of MO_n units (M = V, Mo, or W).[17] Depending on the number of atoms and the combination mode, POMs exhibit diverse structures, including Keggin, Dawson, Anderson, Waugh, and Silver. Notably, Keggin-type POMs ($XM_{12}O_{40}^{n-}$, *e.g.*, $H_3PMo_{12}O_{40}$ and $H_4SiMo_{12}O_{40}$) demonstrate the ability to oxidize and reduce adsorbed substances through a multi-electronic process (ESI Fig. 1†). This rapid multi-electronic redox property provides POMs with an advantage in heterogeneous catalysis. The hybrid systems of immobilized POMs on semiconductors, such as POM-TiO_2[20] and POM-WO_3,[21] presented enhanced photocatalytic performance owing to the effective charge transfer between the two components.

The introduction of POM anions into the interlayer gallery proves to be a simple and effective means of immobilizing POMs. The combination of POM pillared LDHs offers several advantages, including expanded interlayer gallery heights, controlled component losses of POMs in polar solvents, improved specific surfaces of LDHs and POMs, and easy separation and recovery from the reaction.[21] In previous studies, Mg–Al, Zn–Cr, and Zn–Al LDHs pillared by POMs including isopoly-type $W_7O_6^-$, substituted Kegging-type $SiW_{11}O_{39}Mn(H_2O)^{6-}$, and Preyssler-type $NaP_5W_{30}O_{110}^{14-}$ demonstrated noteworthy photocatalytic activity for the degradation of aqueous hexachlorocyclohexane (HCH).[21,22]

Gunjakar *et al.*[23] revealed the mechanism of electron transfer from LDHs to POMs by investigating photocatalytic O_2 generation using isopoly-type $W_7O_{24}^{6-}$ and $V_{10}O_{28}^{6-}$ pillared Zn–Cr LDHs in $AgNO_3$ aqueous solution.

Despite extensive studies on photocatalytic properties, the reliable synthesis of POM pillared LDHs remains a challenge due to the reactivity of some POMs, such as $PW_{12}O_{40}^{3-}$ and $SiW_{12}O_{40}^{4-}$, which react with alkaline LDHs in aqueous solutions instead of forming a hybrid POM/LDH structure. Zhu *et al.*[24] found that the stability of polytungstate increased in aqueous solutions of ethanol or acetone at pH < 8, inspiring our approach to preparing POM pillared LDHs *via* ion exchange in organic solvents at a similar pH to circumvent the reaction between POMs and LDHs.

In this work, we fabricated a Zn–Cr LDH photocatalyst with Keggin-type $SiW_{12}O_{40}^{4-}$ or Keggin-type $H_2W_{12}O_{40}^{6-}$ intercalated into the interlayer gallery *via* ion exchange in an ethanol–water mixed solvent. The photocatalytic activities of CO_2 reduction and O_2 evolution were systematically investigated.

College of Engineering and Applied Sciences, The Frontiers Science Center for Critical Earth Material Cycling, Nanjing University, Nanjing, China. E-mail: miaozhong@nju.edu.cn; jianghy91@nju.edu.cn

† Electronic supplementary information (ESI) available. See DOI: https://doi.org/10.1039/d3na01024d

Results

Zn–Cr LDHs intercalated with NO_3^-, CO_3^{2-}, $SiW_{12}O_{40}^{4-}$, and $H_2W_{12}O_{40}^{6-}$ were denoted as ZCN, ZCC, ZCSW, and ZCHW, respectively. The crystallographic phases of the prepared samples were investigated by X-ray diffraction analysis (XRD) using a Rigaku Ultima IV diffractometer with Cu Kα radiation ($\lambda_{K\alpha1} = 1.540598$ Å, $\lambda_{K\alpha2} = 1.544426$ Å, and Kα2/Kα1 = 0.4970) and D/teX Ultra detector. The Fourier Transform Infrared (FT-IR) spectra of the samples were recorded using a JEOL JIR-7000 at room temperature, with KBr as a reference in the range of 400–4000 cm^{-1}. The morphologies were observed using a JEOL JSM-7600F Schottky field emission scanning electron microscope (SEM) and a Hitachi H8100 transmission electron microscope (TEM). The optical absorption properties of powders were determined by the diffuse reflectance method using a Hitachi U-3310 UV-vis spectrophotometer.

The photocatalytic properties for CO_2 reduction were assessed through a liquid-phase reaction (ESI Fig. 6†). Specifically, 200 mg of the catalyst was dispersed in 50 mL of ultrapure water in a glass reactor with a volume of 290 mL, covered with a quartz window. After degassing with a vacuum pump for 10 min, CO_2 gas was purged into the reactor and flowed for 15 min. Subsequently, the reactor was sealed and positioned beneath one of the two-branched guidance fibers connected to a 200 W Hg–Xe lamp (LA-310UV, Hayashi Watch-works) and irradiated for 24 hours at a light intensity of 15 mW cm^{-2}. The products of CO_2 reduction were analyzed using a gas chromatograph with a flame ionization detector (GC-FID; Shimadzu GC-2014AF equipped with a 1 m ShinCarbon ST 50/80 column and a mechanized apparatus), as well as a gas chromatograph with a thermal conductivity detector (GC-TCD; Shimadzu GC-2014AE equipped with a 6 m ShinCarbon ST 50/80 column).

The photocatalytic properties for water oxidation to O_2 were evaluated by using $NaIO_3$ as a sacrificial agent (ESI Fig. 7†). In detail, 200 mg of catalyst was dispersed in 50 mL ultrapure water in a glass reactor with 290 mL volume, covered with a quartz window. After being degassed with a vacuum pump for 30 min, the sealed reactor was positioned beneath one of the two-branched guidance fibers connected with a 200 W Hg–Xe lamp (LA-310UV, Hayashi Watch-works) and irradiated for 6 hours at a light intensity of 15 mW cm^{-2}. The yield of O_2 was detected with a GC-TCD (Shimadzu GC-2014AE).

Fig. 1b shows the XRD patterns of ZCN and its ion-exchange derivatives ZCC, ZCHW, and ZCSW. For ZCN, the reflections at $2\theta = 9.8°$, 19.8°, and 29.8° are indexed to (003), (006), and (009), indicating a stacked structure of brucite-like layers with an interlayer spacing $d_{003} = 9.00$ Å, consistent with previously reported NO_3^--type LDHs.[19] The reflection at $2\theta = 59.6°$ is assigned to the (110) plane. After ion exchange, for ZCC, the diffraction peaks of (003) and (006) planes are observed at 11.7° and 23.5°, respectively, which have shifted to the wide-angle direction compared to the diffraction peaks of ZCN. Meanwhile, the interlayer spacing has been narrowed down to 7.56 Å, within the range of CO_3^{2-}-type LDHs.[25] The reflection of (009) cannot be well distinguished because it overlaps with the subsequent diffraction peaks. The appearance of the new peaks (101), (015), and (113) indicates that the alkaline environment promoted the growth of LDHs during ion exchange in Na_2CO_3 solution.

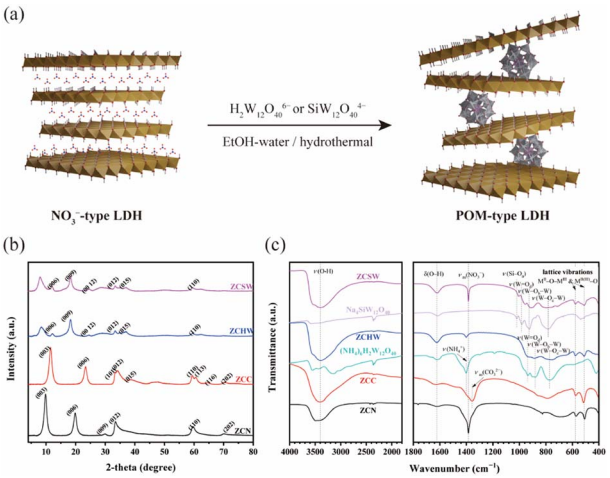

Fig. 1 (a) Illustrated stacking model of LDHs intercalated with simple inorganic anions (NO_3^-) and LDHs pillared by POM ions. (b) XRD patterns of the as-prepared Zn–Cr LDHs intercalated with different inorganic anions. (c) FT-IR spectra of the as-prepared Zn–Cr LDHs intercalated with different inorganic anions.

For POM pillared LDHs, the interlayer spacing can be predicted using the following equation:

$$d_{001} = \frac{l}{3}(D_{POM} + H_{host}) \quad (1)$$

where D_{POM} is the van der Waals diameter of POM ions and H_{host} refers to the thickness of the LDH host layer. In the case of Keggin-type POM ions, D_{POM} is approximately 10 Å, and H_{host} is conventionally 4.8 Å by referring to the value of Mg–Al LDHs as the difference in metal ionic radii between Mg–Al and Zn–Cr is negligible for the host layer thickness. Therefore, the diffraction peaks of (003), (006), and (009) for ZCHW and ZCSW are supposed to be around $2\theta = 6°$, 12°, and 18°, respectively, corresponding to $d_{003} = 15$ Å. According to the XRD results, the peaks are at $2\theta = 12.1°$, 18.3°, and 24.4° for ZCHW and $2\theta = 12.0°$, 18.3°, and 24.5° for ZCSW, which are attributed to the (006), (009) and (0012) planes of reflections, respectively, demonstrating that POM ions entered the interlayer gallery of LDH structures. The peak of (009) exhibits the highest intensity, which differs from the classic LDHs intercalated with simple inorganic anions. However, instead of (003), broad peaks are observed at $2\theta = 8.3°$ for ZCHW and $2\theta = 8.1°$ for ZCSW. Although these phenomena have been reported previously in other types of POM-pillared LDHs, and the reasons for them have not been understood.[26,27] Israëli *et al.*[28] studied the thermodynamics of ion exchange on LDHs and found that the uptake of anions with higher electric density is an entropy-increasing process. Therefore, we suggest that the long-range order structure along the *c*-axis of LDHs was disrupted by the POM intercalation, which disordered the lamellar stacking of LDH host layers. Due to the observation of (110) planes for

POM-pillared LDHs, the structure of brucite-like host layers remained even after ion exchange. The schematic representations of the possible LDH structures before and after ion exchange are displayed in Fig. 1a.

Fig. 1c shows the FT-IR spectra of the as-prepared LDHs and the pristine POMs. In all LDHs, a prominent and broad band is observed around 3400 cm^{-1}, along with a weaker band at 1620 cm^{-1}. These bands correspond to the stretching and bending modes of hydroxyl groups in the LDH host layers and interlayer water molecules, respectively. The peaks in the range of 400–600 cm^{-1} are assigned to the lattice vibrations of Zn–O–Cr or Zn(Cr)–O. For ZCN, the band observed at 1401 cm^{-1} corresponds to the antisymmetric stretching mode of NO_3^- ions. Following ion exchange in ZCC, the vibration peak of NO_3^- was replaced by CO_3^{2-}, observed at 1356 cm^{-1}. In the spectra of ZCHW and ZCSW, the fingerprint peaks of Keggin-type polytungstate appearing at 700–1100 cm^{-1} proved the success of ion exchange, but their positions have been more or less shifted compared with pristine $H_2W_{12}O_{40}^{6-}$ and $SiW_{12}O_{40}^{4-}$, respectively (Table S1†). The position shifts of fingerprint peaks are common in POM-based hybrid composites, usually suggesting interaction between POM ions and other components.[29,30] Here, the peak shifts can be ascribed to the intensive hydrogen-band interaction and the reduced symmetry and freedom degrees in the interlayer gallery. However, the ion exchange with $SiW_{12}O_{40}^{4-}$ was not complete because the vibration peak of NO_3^- remains in the spectrum of ZCSW, although it is much weaker than that in the pristine NO_3^--type LDH. It is probably because the charge densities of the LDH host layer and POM anion are inconsistent. NO_3^- may play an essential role in the accommodation of local charge imbalance by compensating for the excess cationic host layers. Note that although the ion exchange with $H_2W_{12}O_{40}^{6-}$ was processed completely, the presence of NH_4^+, which was the counter-ion of $H_2W_{12}O_{40}^{6-}$ in the pristine polytungstate salt, has been confirmed. NH_4^+ is presumed to act as a compensation of excess POM anions *via* coordination interaction.

Fig. 2 and ESI 9† show the SEM images of all the samples and the EDS-mapping results of POM pillared LDHs. The SEM images displayed the retention of agglomerated, winding, and intertwined plate-like morphology after ion exchange, demonstrating that the introduction of acidic POM molecules did not cause any noticeable damage to the LDH frameworks. From the EDS-mapping analysis, besides the elements zinc and chrome attributed to the host layers, W derived from $H_2W_{12}O_{40}^{6-}$ and Si and W derived from $SiW_{12}O_{40}^{4-}$ are uniformly dispersed in the image regions of ZCHW and ZCSW, respectively, indicating a perfect bond between Zn–Cr host layers and polytungstate anions.

In the TEM images, as shown in ESI Fig. 9,† all the as-prepared LDHs show sheet-like morphologies. The brucite-like layers are preserved after ion exchange. POM clusters were highly dispersed in the interlayer galleries of LDHs. No agglomerated POMs were observed in ZCHW and ZCSW.

ESI Fig. 10† shows the UV-vis diffuse reflection spectra of the as-prepared LDHs. In the UV region, ZCN and ZCC show the

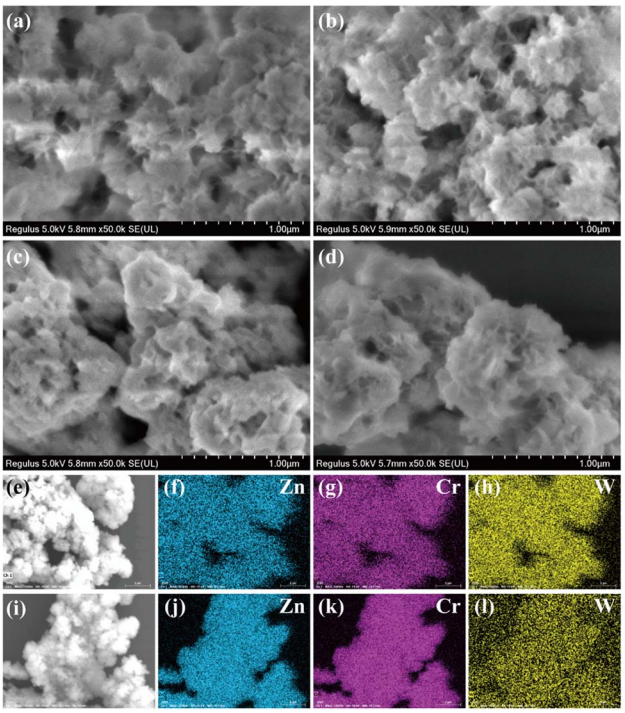

Fig. 2 SEM images of (a) ZCN, (b) ZCC, (c) ZCHW, and (d) ZCSW, and EDS mapping results of (e–h) ZCHW and (i–l) ZCSW.

intrinsic absorption bands of the ligand–metal charge transfer (LMCT) from the O 2p orbital to Zn 4s and Cr 3d orbitals. The absorption fringes at 260 and 318 nm correspond to the band gaps $E_g = 4.8$ eV and 3.9 eV for ZCN and ZCC, respectively. The shoulder peak at 280–320 nm in the spectrum of ZCC is attributed to the metal–metal charge transfer (MMCT) from Cr 3d to Zn 4s,[31] while the weak absorption around 300 nm in the spectrum of ZCN is attributed to the UV excitation of NO_3^- ions. For ZCHW and ZCSW, their intrinsic absorptions have been overlapped by the O 2p → W 5d LMCT of POMs within 400 nm.[32] In addition, the redshifts of Cr^{3+} d–d transition[27] are observed for all the ion-exchanged samples, indicating that interlayer anions influence the electronic structure of host layers.

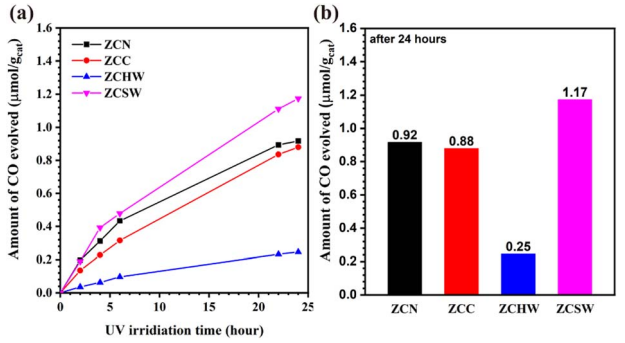

Fig. 3 (a) Time course of CO evolution and (b) total amounts of CO generated after 24 hours for the photo-reduction of CO_2 in water using Zn–Cr LDHs intercalated with various inorganic anions.

Fig. 3 displays the temporal variation of CO generation and the final output in the photo-reduction of CO_2 in pure water using the as-prepared Zn–Cr LDHs intercalated with different kinds of inorganic anions. The CO production over ZCN was 0.92 μmol g^{-1} after 24 hours of UV irradiation. The CO_3^{2-} ion-exchanged sample showed a slightly lower activity, of which the CO production was 0.88 μmol g^{-1}. The disparity in photocatalytic activity is probably owing to the different adsorption characteristics toward CO_2 of the two samples. After being ion-exchanged with $H_2W_{12}O_{40}^{4-}$, the yield of CO dropped sharply to 0.25 μmol g^{-1} after 24 hours, with only 27% of the activity exhibited using the pristine NO_3^--type LDH. This result suggests that the interlayer $H_2W_{12}O_{40}^{4-}$ ions did not function as the reaction sites for the multi-electron reduction of CO_2. In contrast, ZCSW exhibited the highest CO production among all the as-prepared samples, which was 1.17 μmol g^{-1} after 24 hours. Likely, the photo-reduction of CO_2 was promoted due to the host–guest synergistic effect involving charge transfer and the multi-electronic redox ability of $SiW_{12}O_{40}^{4-}$.

For all the as-prepared samples, only trace amounts of CH_4 were detected, while the amount of H_2 generated from water splitting was below the detection limit of the GC-TCD. A blank test was carried out to verify whether CO is derived from CO_2 by repeating UV irradiation toward ZCSW in an Ar atmosphere. The result shows that <0.03 μmol g_{cat}^{-1} of CO was generated after 24 hours, showing that CO was the reduction product of CO_2.

To further investigate the photocatalytic redox properties of POM-pillared LDHs, the photo-oxidation of water for O_2 generation over the as-prepared samples was carried out in a $NaIO_3$ solution. As shown in Fig. 4, ZCN, ZCC, ZCHW, and ZCSW exhibited 65.7, 81.1, 128.0, and 148.1 μmol g^{-1} of O_2 after 6 hour irradiation. The solutions turned pale yellow after the photocatalytic reaction and turned blue after adding starch suspension, indicating the formation of I_2. The slight increase in photocatalytic activity with ZCC is attributed to the band-gap narrowing from the MMCT effect.[30] The enhanced photocatalytic activity with POM-pillared Zn–Cr LDHs toward water oxidation is likely owing to the effective electronic coupling between the semiconductor-like LDH host layers and the catalytically active interlayer species.

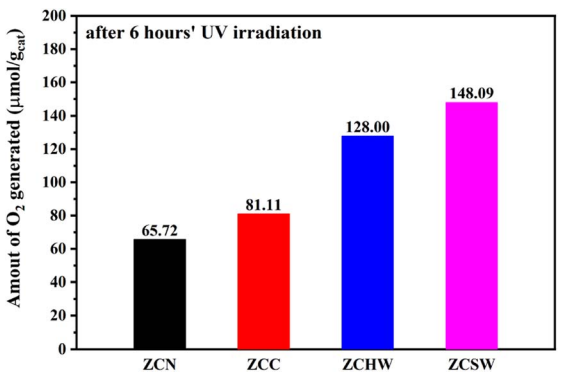

Fig. 4 Total amounts of O_2 generated after 6 hours in $NaIO_3$ aqueous solution for the photo-oxidation of water by using Zn–Cr LDHs intercalated with various inorganic anions.

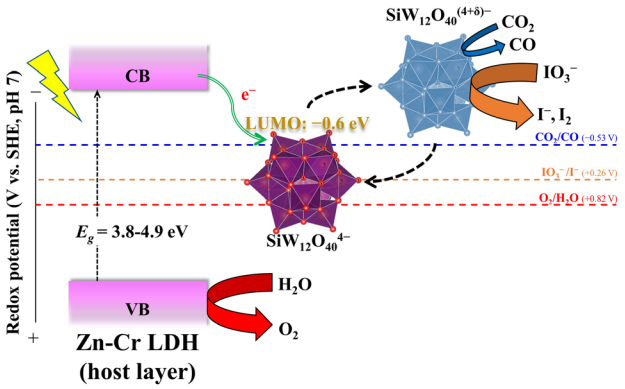

Fig. 5 Possible mechanism and charge transfer route between LDH host layers and POM anions in the photo-reduction of CO_2 and photo-oxidation of water.

In previous work, Nakajima *et al.*[33] reported charge transfer in polytungstate-TiO_2 hybrids. The photo-generated electrons in the CB of anatase transferred to the LUMO and HOMO of polytungstate. Similar to anatase, Zn–Cr LDH host layers also inject the photo-generated electrons to the LUMO and HOMO of POMs to realize charge separation. In the case of ZCSW, the data of half-wave potentials for the 1-electron reduction reported indicated the LUMO of $SiW_{12}O_{40}^{4-}$ lies at −0.6 eV (pH = 7), which can withstand the reduction of CO_2 and IO_3^-.[34] However, $SiW_{12}O_{40}^{4-}$ is likely more favorable to reduce IO_3^- than CO_2 because of the more significant potential drop between the LUMO energy and the reduction potential (Fig. 5). Due to the pseudo-liquid phase and multi-electron redox properties, IO_3^- can freely enter or leave the framework of POMs and be rapidly reduced without barriers in the reaction kinetics.

Conclusions

In this work, Zn–Cr LDH photocatalysts were prepared. Keggin-type polyanion $SiW_{12}O_{40}^{4-}$ and $H_2W_{12}O_{40}^{6-}$ pillared Zn–Cr LDHs (ZCHW and ZCSW) were synthesized through ion exchange using a NO_3^--type LDH (ZCN) as the raw material. In the photo-reduction of CO_2, ZCSW produced up to 1.17 μmol g^{-1} CO after 24 hour UV irradiation, which was 1.2-fold higher than that of ZCN. In the photo-oxidation of water in the presence of IO_3^-, ZCSW produced up to 148.1 μmol g^{-1} O_2 after 6 hour irradiation, which was 2.2-fold higher than that of ZCN. The results of characterization and mechanistic investigations indicated that the electron transfer from the conduction band of the Zn–Cr LDH to the lowest unoccupied molecular orbital (LUMO) of $SiW_{12}O_{40}^{4-}$ probably contributes to the enhanced photocatalytic activity in CO_2 reduction and water oxidation.

Conflicts of interest

There are no conflicts to declare.

Acknowledgements

This work was supported by the National Natural Science Foundation of China (grant number 22272078) and the Frontiers Science Center for Critical Earth Material Cycling of Nanjing University.

Notes and references

1 G. Mishra, B. Dash and S. Pandey, *Appl. Clay Sci.*, 2018, **153**, 172–186.
2 K. Teramura, S. Iguchi, Y. Mizuno, T. Shishido and T. Tanaka, *Angew. Chem., Int. Ed.*, 2012, **51**, 8008–8011.
3 S. Iguchi, K. Teramura, S. Hosokawa and T. Tanaka, *Phys. Chem. Chem. Phys.*, 2015, **17**, 17995–18003.
4 L. Li, Z. Liu, X. Yu and M. Zhong, *Angew. Chem., Int. Ed.*, 2023, **62**, e202300226.
5 S. Iguchi, K. Teramura, S. Hosokawa and T. Tanaka, *Appl. Catal., A*, 2016, **521**, 160–167.
6 H. Jiang, K. Katsumata, J. Hong, A. Yamaguchi, K. Nakata, C. Terashima, N. Matsushita, M. Miyauchi and A. Fujishima, *Appl. Catal., B*, 2018, **224**, 783–790.
7 H. Jiang, L. Wang, H. Kaneko, R. Gu, G. Su, L. Li, J. Zhang, H. Song, F. Zhu, A. Yamaguchi, J. Xu, F. Liu, M. Miyauchi, W. Ding and M. Zhong, *Nat. Catal.*, 2023, **6**, 519–530.
8 L. Li, A. Ozden, S. Guo, F. P. García de Arquer, C. Wang, M. Zhang, J. Zhang, H. Jiang, W. Wang, H. Dong, D. Sinton, E. H. Sargent and M. Zhong, *Nat. Commun.*, 2021, **12**, 5223.
9 X. Xiong, Y. Zhao, R. Shi, W. Yin, Y. Zhao, G. I. N. Waterhouse and T. Zhang, *Sci. Bull.*, 2020, **65**(12), 987–994.
10 X. Xiong, C. Mao, Z. Yang, Q. Zhang, G. I. N. Waterhouse, L. Gu and T. Zhang, *Adv. Energy Mater.*, 2020, **10**, 2002928.
11 Y. Zhao, G. Chen, T. Bian, C. Zhou, G. I. N. Waterhouse, L.-Z. Wu, C.-H. Tung, L. J. Smith, D. O'Hare and T. Zhang, *Adv. Mater.*, 2015, **27**, 7824–7831.
12 G. Huang, Q. Niu, J. Zhang, H. Huang, Q. Chen, J. Bi and L. Wu, *Chem. Eng. J.*, 2022, **427**, 131018.
13 M. Liu, G. Zhang, X. Liang, Z. Pan, D. Zheng, S. Wang, Z. Yu, Y. Hou and X. Wang, *Angew. Chem., Int. Ed.*, 2023, **62**, e202304694.
14 M. Hao, D. Wei and Z. Li, *Energy Fuels*, 2022, **36**(19), 11524–11531.
15 B. Su, M. Zheng, W. Lin, X. F. Lu, D. Luan, S. Wang and X. W. D. Lou, *Adv. Energy Mater.*, 2023, **13**, 2203290.
16 C. G. Silva, Y. Bouizi, V. Fornés and H. García, *J. Am. Chem. Soc.*, 2009, **131**, 13833–13839.
17 Y. Zhao, B. Li, Q. Wang, W. Gao, C. J. Wang, M. Wei, D. G. Evans, X. Duan and D. O'Hare, *Chem. Sci.*, 2014, **5**, 951–958.
18 Y. Wu, M. Song, Y.-C. Huang, C.-L. Dong, Y. Li, Y. Lu, B. Zhou, D. Wang, J. Jia, S. Wang and Y. Wang, *J. Energy Chem.*, 2022, **74**, 140–148.
19 J. L. Gunjakar, T. W. Kim, H. N. Kim, I. Y. Kim and S.-J. Hwang, *J. Am. Chem. Soc.*, 2011, **133**, 14998–15007.
20 Y. Guo, Y. Wang, C. Hu, Y. Wang, E. Wang, Y. Zhou and S. Feng, *Chem. Mater.*, 2000, **12**, 3501–3508.
21 Y. Guo, D. Li, C. Hu, Y. Wang and E. Wang, *Int. J. Inorg. Mater.*, 2001, **3**, 347–355.
22 A. Miyoshi, Y. Shimoyama, H. Mogi, H. Ubukata, N. Hirayama, A. Tanaka, K. Arai, S. Morita, T. Yui, S. Uchida, T. Motohashi, Y. Inaguma, H. Kageyama and K. Maeda, *Chem. Lett.*, 2022, **51**, 107–110.
23 J. L. Gunjakar, T. W. Kim, I. Y. Kim, J. M. Lee and S.-J. Hwang, *Sci. Rep.*, 2013, **3**(1), 2080.
24 Z. Zhu, R. Tain and C. Rhodes, *Can. J. Chem.*, 2003, **81**, 1044–1050.
25 K. Parida and L. Mohapatra, *Dalton Trans.*, 2012, **41**, 1173–1178.
26 S. Yanagida, A. Nakajima, Y. Kameshima and K. Okada, *J. Ion Exch.*, 2007, **18**(4), 270–275.
27 T. Takei, A. Miura and N. Kumada, *J. Australas. Ceram. Soc.*, 2014, **2**, 289–296.
28 Y. Israëli, C. Taviot-Guého, J.-P. Besse, J.-P. Morel and N. Morel-Desrosiers, *J. Chem. Soc., Dalton Trans.*, 2000, 791–796.
29 X. Jing, D. Zou, Q. Meng, W. Zhang, F. Zhang, W. Feng and X. Han, *Inorg. Chem. Commun.*, 2014, **46**, 149–154.
30 A. Lesbani, A. Agnes, R. O. Saragih, M. Verawaty, R. Mohadi and H. Zulkifli, *Bull. Chem. React. Eng. Catal.*, 2015, **10**, 185–191.
31 N. Baliarsingh, L. Mohapatra and K. Parida, *J. Mater. Chem. A*, 2013, **1**, 4236–4243.
32 Y. Chen, G. Yu, F. Li, C. Xie and G. Tian, *J. Mater. Chem. C*, 2013, **1**, 3842–3850.
33 K. Pruethiarenun and A. Nakajima, *J. Jpn. Soc. Colour Mater.*, 2014, **87**, 227–234.
34 J. Zhang, C. Guo, S. Fang, X. Zhao, L. Li, H. Jiang, Z. Liu, Z. Fan, W. Xu, J. Xiao and M. Zhong, *Nat. Commun.*, 2023, **14**, 1298.